Inorganic Chemistry

Article

pubs.acs.org/IC

Metal and Metal Carbide Nanoparticle Synthesis Using Electrical Explosion of Wires Coupled with Epoxide Polymerization Capping

Elseddik M. Abdelkader, Paul A. Jelliss,* and Steven W. Buckner*

Department of Chemistry, Saint Louis University, St. Louis, Missouri 63103, United States

Supporting Information

ABSTRACT: In this study, metal-containing nanoparticles (NPs) were produced using electrical explosion of wires (EEW) in organic solvents. The explosion chamber was constructed from Teflon to withstand the shockwave, allow growth and reaction of the incipient NPs in various organic solvents containing dissolved ligands, and allow a constant flow of argon to maintain an inert environment. A survey of different transition d-block metals was conducted with metals from groups 4−8, affording metal carbide NPs, while metals from groups 9−12 gave elemental metallic NPs. Tungsten carbide phase WC_{1-x}, which has not been previously isolated as a single-phase material, was exclusively formed during EEW. We used polymerization initiation by electron-rich metallic nanoparticles (PIERMEN) as a capping technique for the nascent NPs with an alkyl epoxide employed as the monomers. Transmission electron microscopy showed spherical particles with the metallic core embedded in a polymer matrix with predominantly smaller particles (<50 nm), but also a broad size distribution with some larger particles (>100 nm). Powder X-ray diffraction (PXRD) was used to confirm the identity of the metallic NPs. The capping agents were characterized using ATR-FTIR spectroscopy. No evidence is observed for the formation of crystalline oxides during EEW for any metals used. Differential scanning calorimetry/thermal gravimetric analysis was used to study the NP's behavior upon heating under an air flow up to 800 °C with the product oxides characterized by PXRD. The bifurcation between metal-carbide NPs and metal NPs correlates with the enthalpy of formation of the product carbides. We observed PIERMEN capping of elemental metal NPs only when the metal has negative standard electrode potentials (relative to a bis(biphenyl) chromium(I)/(0) reference electrode).

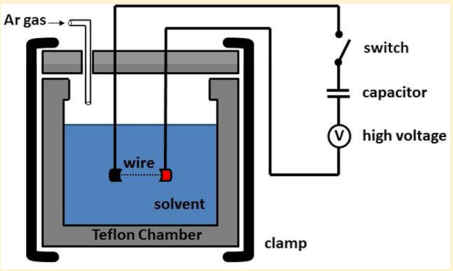

INTRODUCTION

Metal carbides are known for their high melting points, superior corrosion and wear resistance, good catalytic properties, and electronic properties.[1] These metal carbides, known as refractory compounds, are used for cutting tools and also as structural materials due to their high chemical stability and thermal conductivity.[2] Synthesis of metal carbides can be carried out by reaction of the elements at high temperatures, which is usually associated with long times, high energy usage, and incomplete conversions. Other synthetic routes include chemical vapor condensation,[3] electrochemical synthesis,[4] sonochemistry,[5] carbothermal synthesis,[6] and electrical explosion of wires (EEW).[7] EEW, or what is sometimes called pulsed wire discharge (PWD),[8] was first described in 1774 and later led to many applications such as exploding wire detonators,[9] explosion current interrupters,[10] high-temperature process photography,[11] and nanoparticle (NP) production, which was first used for materials synthesis in 1946.[12] EEW consists of a capacitor bank that discharges high current (10^4−10^6 A/mm^2) through a wire of the desired material in a short time (10^{-8}−10^{-5} s). This quantity of energy is much larger than the sublimation energy of the wire, which leads to superheating, evaporation, and scattering of wire material into the surrounding medium, followed by condensation of the vapor to form nanoparticles.[13] The process is also accompanied by a shock wave generation and a bright flash of light prior to expansion of boiling wire droplets and vapor to the surroundings. EEW has been used for production of metals,[14−16] metal oxides,[17,18] metal nitrides,[19,20] alloys,[21,22] nanocomposites,[23] and metal carbides[24] in addition to fullerenes[25] and carbon nanotubes.[26] This method has been applied in gaseous,[27] aqueous,[28] and organic media.[29] However, EEW cannot be used for organometallics or thermally labile hydrides due to their limited thermal stability and possible competing pyrolysis reactions of hydrocarbons.[30]

Ilyin et al. have synthesized titanium, tungsten, tantalum, and aluminum carbides in both liquid and gas phase media.[31] They showed that gaseous media (acetylene, propane, or a mixture of them with argon) gave residual metal and carbon-deficient carbides. Increasing the output of carbides can be accomplished using either higher gas pressure (which is not always technically possible) or more dense media such as liquid hydrocarbons (hexane, benzene, toluene, or decane) where the concentration of carbon atoms is higher compared to gases. They used wires of 0.2−0.5 mm diameter and 5−12 cm length associated with 12.5−30 kV charging voltage and 1−5 μF capacitance.

Metal NPs have many applications including DNA sensing,[32] fuel cells,[33] and catalysis.[34] They also have applications in reactive energetic materials. EEW synthesis of metal NPs has

Received: March 27, 2015
Published: May 26, 2015

DOI: 10.1021/acs.inorgchem.5b00697
Inorg. Chem. 2015, 54, 5897−5906

many advantages.[35] First, it is a relatively simple technique. It is also a general method that is applicable to any metal that can form stable and low-diameter wires. Finally, EEW is relatively clean with minimal side-product formation.

In this study, we investigated the production of metal NPs of 14 d-block elements using EEW as a clean, environmentally friendly, and economical technique. This provided an opportunity to evaluate the applicability of polymerization capping using epoxide ligands for a variety of different metal NPs (polymerization initiation by electron-rich metallic nanoparticles (PIERMEN)). During this process we found an interesting bifurcation in the production of metal versus metal carbide NPs in the EEW process.

EXPERIMENTAL METHODS

Reagents and Materials. Toluene (anhydrous, 99.8%), 1,2-epoxydodecane, benzene, and tetrahydrofuran (THF) were purchased from Sigma-Aldrich. Acetonitrile and diethylenetriamine were purchased from Fisher Scientific. Hexanes (mixture of isomers) were purchased from Macron Fine Chemicals. Wires (0.25 mm diameter, ≥98% metals basis) of zinc, copper, nickel, cobalt, iron, molybdenum, niobium, titanium, tungsten, zirconium, hafnium, silver, palladium, and vanadium were purchased from Alfa Aesar. Tantalum wire (0.25 mm diameter, 99.95%) was purchased from Strem Chemicals. Solvents were purified and dried by distillation over molecular sieves.

Synthesis. The chamber used for EEW was described previously.[36] Figure S1 shows the main parts of the experiment along with the explosion chamber. The chamber was subjected to argon flow for 5–10 min to provide an oxygen-free atmosphere during the explosion. It was also connected to a bubbler to avoid overpressure problems. The storage capacitance is 96 μF, and the voltage prior to discharge varies between 4.0 and 4.4 kV. The capacitors are connected to the chamber feedthroughs via a spark gap switch. After the first explosion, the wire can be fed manually to start another discharge or up to three wires can be exploded simultaneously. Generally, greater than 85% of the wires were exploded into NPs, leaving the rest as small metallic pieces. After the explosion, the reaction solution and the freshly produced and capped particles are transferred to a Schlenk tube, where the solvent was evaporated *in vacuo* followed by overnight drying.

Characterization. Dried NPs were suspended in toluene to be used for characterization by transmission electron microscopy (TEM) on a JEOL 1200 instrument. Samples were cast on Formvar grids provided by Ted Pella. ATR-FTIR (attenuated total reflectance-Fourier transform infrared) spectra were obtained using a Shimadzu model FTIR-8400S spectrometer. Spectra were collected using the solid directly without dissolution in a solvent. Powder X-ray diffraction (PXRD) was carried out using a Rigaku Miniflex 600 X-ray diffractometer with Cu Kα radiation (40 kV, 15 mA) with a scan rate of 1 °C/min. The presence of different metal and metal carbides was confirmed by comparisons with the appropriate patterns from the ICDD Crystallographic Database. Thermal analysis by differential scanning calorimetry (DSC) and thermal gravimetric analysis (TGA) was performed with a TA Instruments SDT Q600 simultaneous DSC/TGA. The samples were heated to 800 °C with a 10 °C/min temperature ramp under a constant 10–20 mL/min flow of air using platinum cups.

RESULTS

Metal nanopowder production has many industrial and technological applications. We chose 14 different metals for testing with EEW coupled with PIERMEN to investigate the different results of this synthetic protocol. Toluene was the solvent used for all metals prior to comparison with other solvents. All nanomaterial products are black powders that are well dispersed in the solvent for 15–40 min before settling out of solution.

Late Transition Metals. Transition metal NPs with a high percentage of atoms on the surface are of great importance in catalytic processes such as hydrogenation, hydrocracking, and aromatization.[37] Synthesis of these metal NPs can be carried out by electrochemical methods,[38] organometallic synthesis,[39] surface redox reactions,[40] and the polyol process.[41] EEW also was employed to produce zinc NPs by our group using different liquids with diameters of around 100 nm.[36] Yilmaz et al.[42] produced cobalt NPs by EEW in a nitrogen atmosphere with resulting NP sizes below 50 nm. Their circuit consisted of a 6 μF capacitor and 24–28 kV charge voltage for wires of 50 mm length and 0.6 mm diameter. They showed that increasing the charging voltage leads to decreasing particle size and increasing number of single-crystalline particles relative to the polycrystalline ones.

In this report, five d-block pure metallic NPs were produced including Co, Ni, Cu, Pd, and Ag. PXRD patterns of cubic cobalt and nickel NPs as an example of late transition metals are shown in Figure 1 with no oxide or carbide phases

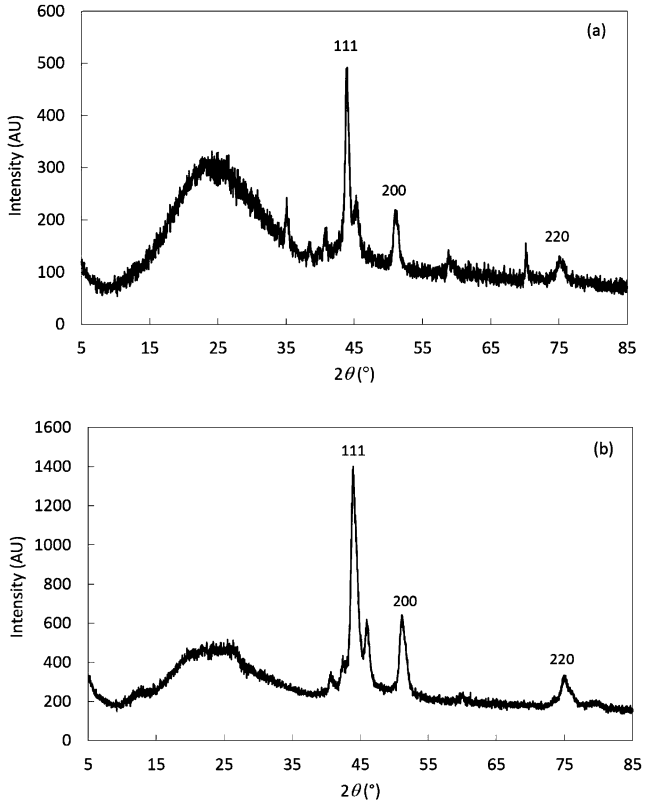

Figure 1. PXRD patterns of (a) Co (PDF# 01-071-4238) NPs and (b) Ni (PDF# 01-077-9326) NPs capped with 1,2-epoxydodecane.

observed. Scherrer analysis of the peak widths for Ni and Co indicates relatively small crystallite diameters of 9 and 11 nm, respectively (Table 1). Of the remaining late d-block metals, only Pd NPs (11 nm) compare with these dimensions. Those of Ag (16 nm) and Cu (29 nm), in particular, are larger. Values previously observed for Zn (17 nm)[36] in our EEW work are intermediate between these two extremes, similar to those of Ag. PXRD patterns of Ag, Cu, and Pd NPs are shown in the Supporting Information (Figures S2 and S3). TEM micrographs were also used to characterize the NPs as shown in Figure 2. The sizes shown appear to be less than 50 nm, a value that includes an oligomerized epoxide capping layer as well as

DOI: 10.1021/acs.inorgchem.5b00697
Inorg. Chem. 2015, 54, 5897–5906

Table 1. Diameters of Metallic NP Crystallites Produced by EEW As Determined by Scherrer Analysis of Peaks in PXRD Patterns

metal	crystallite diameter (nm)
Co	11
Ni	9
Cu	29
Pd	11
Ag	16

the metal NP core itself. However, we can see agglomeration of larger sized particles as well, although still less than 100 nm. This further confirms the advantage of using liquid media for EEW to suppress the plasma around the wire's surface, leading to enhancement of energy deposition and hence formation of NPs with very small diameters.

Thermal analysis of the late transition metal NPs was investigated using DSC/TGA as seen in Figure 3 for Ni NPs as an example. When nickel NPs underwent heating up to 400 °C, we observed three small exothermic peaks associated with a weight decrease due to loss of carbon dioxide as a result of oxidation of the organic cap and the amorphous carbon. Around 500 °C we can see a broader exothermic peak associated with a very slight weight gain (detectable only above 550 °C) that can be attributed to formation of nickel(II) oxide, NiO, which is confirmed by PXRD analysis (with peaks at 2θ 37.4°, 43.4°, and 62.8°), as shown in Figure 4. Even though we have very small size NPs according to Scherrer analysis, the weight gain is not as high as was reported previously.[43] Generally, decreasing NP size leads to an increase of the oxidation rate due to the larger surface area and more complete oxidation.

Nevertheless, and despite their small size, this behavior could be attributed to incomplete oxidation of the NPs, and indeed we can see weak Ni peaks (44.6° and 52.0°) in the post DSC/TGA PXRD pattern in Figure 4. Also, the amount of nickel compared with the amount of combusted cap and amorphous carbon can be very small, as EEW produces significant amounts of carbon due to solvent pyrolysis.[36] Similar behavior was observed for other metals except silver, which did not oxidize.

Early Transition Metals. EEW has been previously used to synthesize many materials, including metals and metal carbides, both directly and indirectly. Tungsten carbide was synthesized indirectly by Aravinth et al.,[44] who produced tungsten/tungsten oxide by EEW followed by carburization of the particles with multiwalled carbon nanotubes (MWCNTs). They carried out the explosion in an argon/oxygen mixture followed by mixing the NPs with MWCNTs and heating at 1250 °C for 7 h to form simple spherical hexagonal α-WC particles with 19 nm average diameters.

EEW can cause thermal dissociation of an organic liquid medium, leading to liberation of carbon atoms, which can react with the metal atoms produced to form metal carbides.[31] Carbides form when the explosion temperature decreases to a thermodynamically possible extent for the reaction to proceed: 3000−4000 °C above which chemical dissociation dominates, while below 300−400 °C diffusion rates become minimal. While the rate of product cooling is very high after the explosion (10^8 °C/s), in the area of chemical reaction (3000−4000 °C) it is relatively low (10^3 °C/s), which makes it possible to use thermodynamic analysis for the reactions.

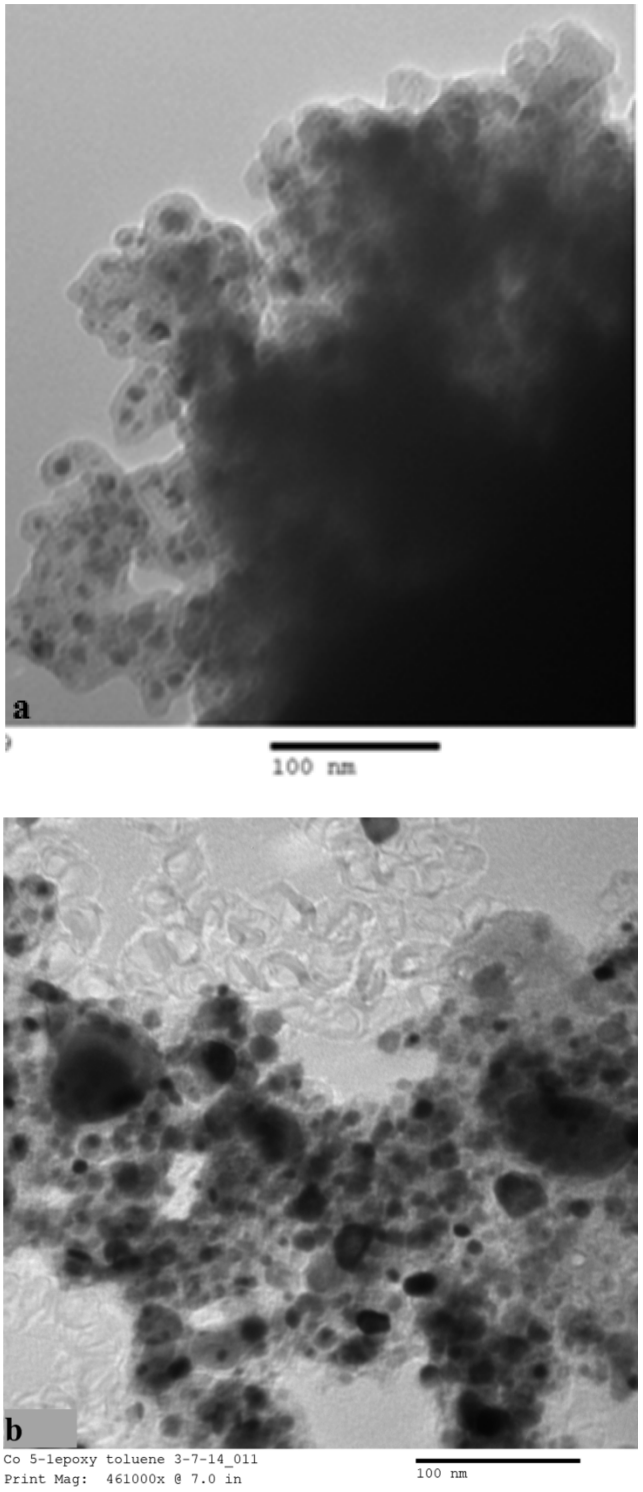

Figure 2. TEM micrographs of (a) Ni NPs and (b) Co NPs capped with 1,2-epoxydodecane in toluene.

In this work, we tried to synthesize transition metals other than the ones characterized above, but we find that for early transition metals we form only metal carbides. Our data show that early transition d-block metals (groups 4−8) gave metal carbides, while late transition metals (groups 9−12) gave elemental metallic NPs as described above. We used PXRD to confirm the carbide phases of products as shown in Figure 5 for the cubic hafnium carbide (HfC) and the monoclinic iron carbide (Fe_5C_2) as examples with average diameters of 15 and 8

DOI: 10.1021/acs.inorgchem.5b00697
Inorg. Chem. 2015, 54, 5897−5906

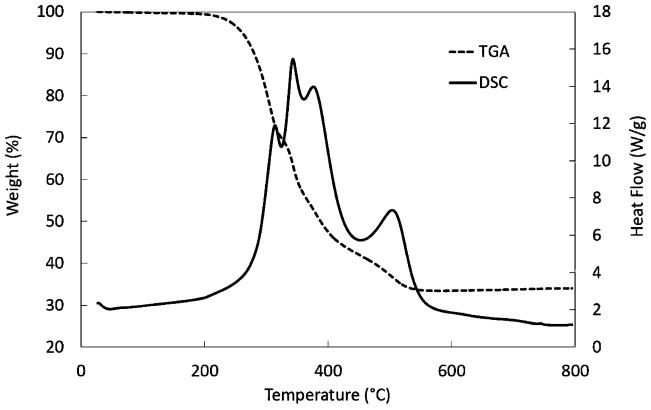

Figure 3. DSC/TGA profiles of Ni NPs produced by EEW.

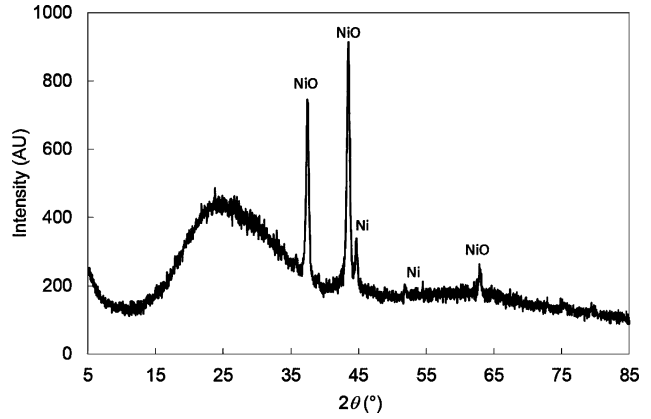

Figure 4. PXRD of NiO (PDF# 00-047-1049) after heating of Ni NPs in DSC/TGA analysis.

nm, respectively (Table 2). PXRD of the rest of the metal carbides is shown in the Supporting Information (Figures S4–S6).

Either C–H activation by metals, decarburization of the capping agent, or solvent pyrolysis could be the source of carbon in the carbide formation process. Toluene can be catalytically activated by metals via C–H activation to form carbides in a similar fashion to methane.[45] To test these possibilities, we used benzene as a solvent, and we found that it also produced carbides as well with similar sizes to those formed in toluene. Formation of metal carbides was not the result of using an epoxide as a capping agent either. In the absence of the epoxide, the uncapped metals from groups 4–8 gave carbide NPs and metals from groups 9–12 gave metallic NPs. Therefore, formation of carbon atoms simply comes from the pyrolysis of the solvent itself, which can combine with metallic atoms to form the carbides. We have shown previously that EEW causes local reaction temperatures to be high enough (reaching 3000 °C) to pyrolyze the solvent.[36]

Alternatively, hot atoms and ions produced in the initial exploding wire plasma may react rapidly with solvent and cap molecules via C–H and C–C insertion to form small, carbon-rich molecular fragments. Armentrout has extensively studied the reactions of both kinetically and electronically excited atomic metal ions.[46–48] These studies show formation of metal carbides for a variety of saturated organic molecules reacting with metal ions. Direct ring cleavage reactions of benzene and pyridine have been reported, forming smaller metal-bound C_2 and C_4 structures.[49,50] Also, early transition metal ions are

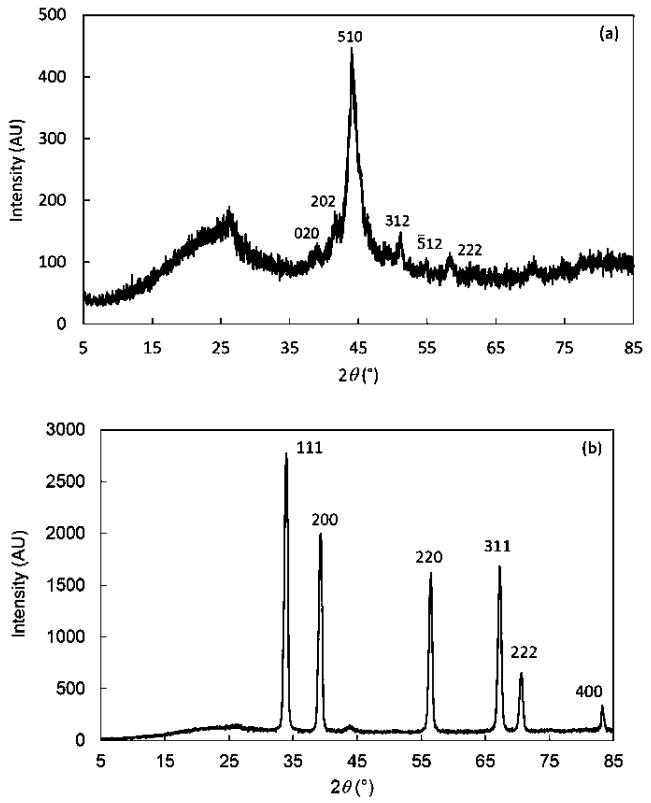

Figure 5. PXRD patterns of (a) Fe_5C_2 (PDF# 01-089-8968) NPs and (b) HfC (PDF# 01-076-7072) NPs formed by EEW in toluene.

Table 2. Diameters of Metal Carbide NP Crystallites Produced by EEW As Determined by Scherrer Analysis of Peaks in PXRD Patterns

carbide phase	crystallite diameter (nm)
TiC	17
VC	23
Fe_5C_2	8
ZrC	22
NbC	16
MoC	20
HfC	15
TaC	30
WC_{1-x}	14

particularly reactive and are known to react with multiple organic molecules by dehydrogenation followed by effective ligand coupling to form larger fused ring systems.[51–53] These fused ring systems can also undergo dehydrogenation at elevated energies to form atomic metal carbide structures. Thus, reactions between solvent and cap molecules and the excited atoms and ions produced in the initial explosion may contribute to the formation of metal carbides.

In their study, Ilyin et al. showed that increasing the C/H ratio leads to increasing the output of metal carbides and decreasing the metal content. We attempted to synthesize metallic NPs by decreasing the number of carbons from toluene to benzene, hexane, diethylenetriamine, and finally acetonitrile. However, metal carbide NPs were still formed for early transition metals and metallic NPs for late transition metals. Changing experimental conditions such as lowering the voltage down to 1.4 kV and using a solvent vortex (to avoid full

DOI: 10.1021/acs.inorgchem.5b00697
Inorg. Chem. 2015, 54, 5897–5906

immersion in the liquid) also gave the same results. TEM was also used to characterize the carbide NPs as shown in Figure 6.

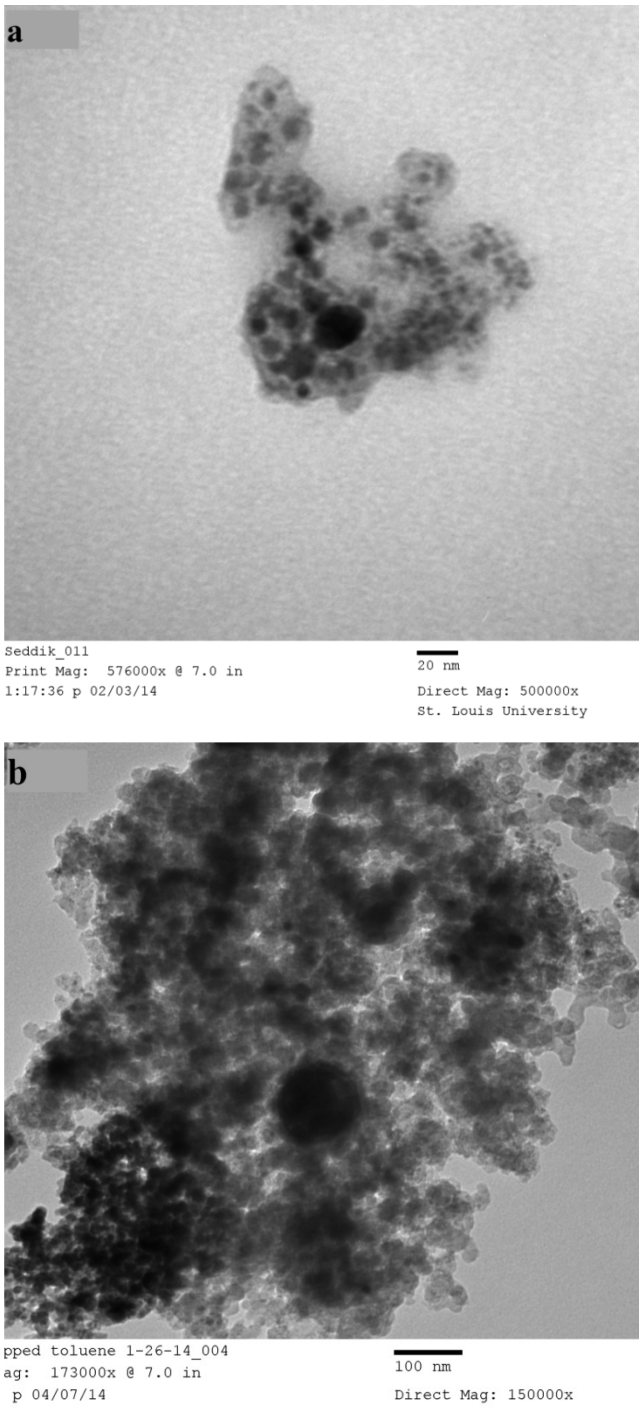

Figure 6. TEM micrographs of (a) Fe_5C_2 NPs capped with 1,2-epoxydodecane and (b) TiC NPs (no epoxide) formed by EEW in toluene.

We can see that the organic polymer matrix is similar to that observed for the metallic NPs. Figure 6b shows the TEM analysis for the darker titanium carbide NPs surrounded by the lighter matrix most likely of the amorphous carbon from the solvent pyrolysis.[36]

In our synthesis, we formed nonstoichiometric carbides with iron and also with tungsten, as shown in Figures 5 and 6. In previous synthetic methods such as that described by Ilyin and Nazarenko,[54] the phase WC_{1-x} has always been synthesized among other phases. They reported the synthesis of different metal carbides (TiC, Al_4C_3, WC, W_2C, and WC_{1-x}) in different hydrocarbons (benzene, toluene, hexane, decane, hexamethylenetetramine suspended in decane and solid paraffin). They showed that higher density, dynamic viscosity, and C/H ratio of hydrocarbons lead to higher output of tungsten carbides and a lower amount of residual metal. In this previous work, hexagonal closed-packed (hcp) tungsten carbide W_2C is formed in liquid phase at temperatures over its melting point (3130 K) by diffusion of carbon atoms into the liquid W particles (eq 1). The phase W_2C has polymorphs (β, α, γ, ε) that differ in ordering degrees of carbon atoms in the octahedral vacancies of tungsten atoms.

$$2W(l) + C(g) \rightarrow W_2C(l) \quad (1)$$

However, most of the carbide was formed with the fcc structure β-WC or what is called WC_{1-x}, which has a high thermal stability above 2800 K with $0 \leq x \leq 0.41$ due to a high concentration of carbon atoms and quick cooling of particles. Higher C/H ratios lead to higher percentages of WC_{1-x} compared to W_2C. The phase α-WC is formed only when the solid paraffin was used.

We saw a similar behavior when we used tungsten in toluene, but the phase WC_{1-x} was formed exclusively and in the absence of any other tungsten carbide phases at all. The formation of this carbon-deficient phase was confirmed by PXRD analysis, as shown in Figure 7, and occurs irrespective of the presence of epoxydodecane as a capping agent (Figure S7, Supporting Information).

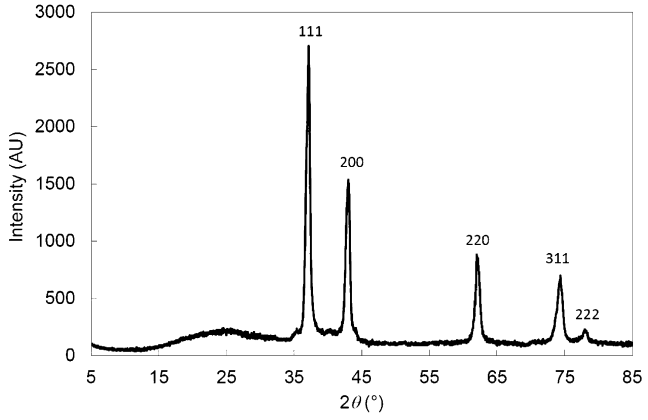

Figure 7. PXRD pattern of WC_{1-x} (PDF# 00-020-1316) NPs capped with 1,2-epoxydodecane.

Ilyin and Nazarenko reported an EEW capacitance and charging voltage of 1.2 μF and 15−30 kV, respectively. On the basis of these parameters, the maximum deliverable energy to the tungsten wire ($E = 1/2CV^2$) was 540 J. With a capacitance that is much higher (96 μF) and despite a lower charging voltage (4.4 kV maximum) our EEW is capable of delivering larger energies (ca. 930 J) in a comparable time frame and thus is expected to generate a higher localized plasma temperature. This would account for the formation of the observed WC_{1-x} phase exclusively in our work.

TEM was used to characterize the morphology of our WC_{1-x} NPs as shown in Figure 8. We can see that they appear to be much smoother and more spherical compared with the other

DOI: 10.1021/acs.inorgchem.5b00697
Inorg. Chem. 2015, 54, 5897−5906

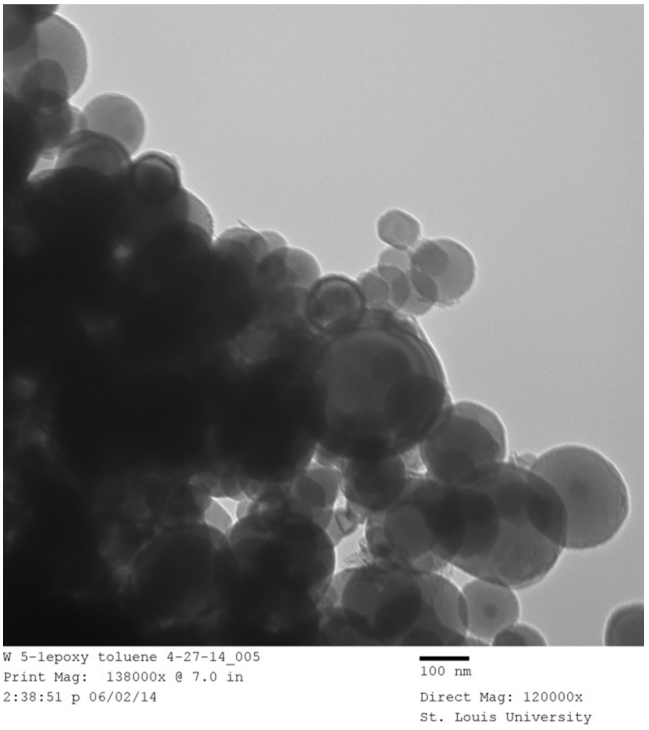

Figure 8. TEM micrograph of WC_{1-x} NPs capped with 1,2-epoxydodecane.

carbide and metal NPs produced in this work. Similar observations were made by Ilyin and Nazarenko, although their previously reported multiphasic tungsten carbide NPs, though spheroidal, were not as smooth as the tungsten carbide produced in this report.

The crystallite NP diameter, as shown in Table 2, of this phase was 14 nm according to Scherrer analysis of the PXRD peak widths. However, we can see the larger sizes up to 200 nm in the TEM micrographs. This is in part due to the broad size distribution but can also be attributed to the capping agent around the crystalline NP cores. When epoxydodecane is not used in the EEW solvent, the NP diameter is observed to be similarly small at 11 nm.

The thermal behavior of the metal carbide NPs was investigated using DSC/TGA. As an example, WC_{1-x} behavior is shown in Figure 9. Similar to metal NPs, loss of the organic

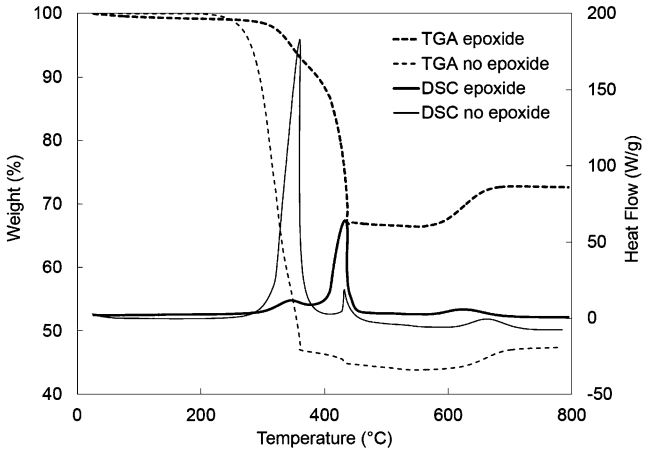

Figure 9. DSC/TGA profiles of WC_{1-x} NPs produced by EEW.

cap and amorphous carbon was followed by a slight weight gain to give the corresponding oxides. However, the weight gain is more pronounced than metal NPs as shown earlier. PXRD of the oxide product is shown in Figure 10 and verifies that there is no tungsten carbide WC_{1-x} phase remaining at all, with WO_3 identified as the only recognizable phase (eq 2).

$$WC_{1-x}(s) + \frac{3 + 2(1 - x)}{2}O_2(g) \rightarrow WO_3(s) + (1 - x)CO_2(g) \quad (2)$$

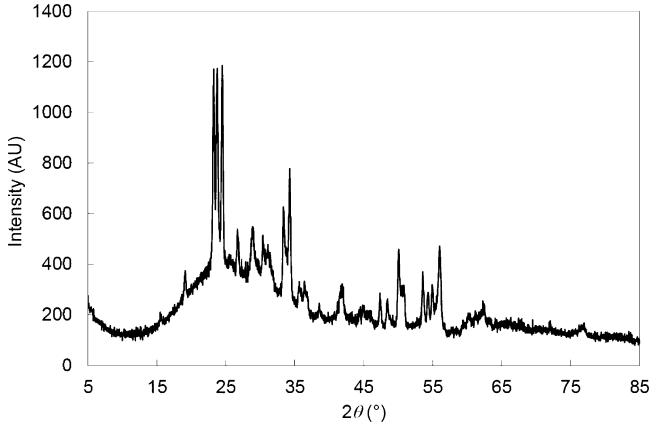

Figure 10. PXRD pattern of WO_3 (PDF# 00-043-1035) after DSC/TGA analysis of WC_{1-x} NPs.

There are subtle differences in the thermal profiles for WC_{1-x} depending on whether epoxydodecane is incorporated. In the absence of the epoxide, the majority of the mass loss (53%) occurs in the range 230−370 °C, coincident with a sharp exotherm at 360 °C. This is followed by a considerably smaller exotherm at 430 °C with a much smaller mass loss (2%) from 370 to 420 °C. The oxidation onset for the WC_{1-x} cores begins at 563 °C. If epoxide is incorporated into the EEW synthesis, the same mass losses and exotherms occur at the same temperatures, but are reversed in relative magnitude. Thus, the dominant exotherm at 430 °C is accompanied by the majority of the mass loss from 370 to 420 °C. Additionally the WC_{1-x} oxidation onset temperature is slightly higher (600 °C).

In the absence of epoxydodecane the principal source of capping material must be the solvent, toluene, which is being pyrolyzed to afford amorophous carbon, likely in the form of graphitic sheets on the WC_{1-x} NP surface (Figure 11a). These sheets presumably adhere to the NP surface by the action of dispersion forces and are partially removed by oxidation corresponding to the lower temperature mass loss and exotherm at 360 °C. With epoxydodecane present in solution during EEW, we hypothesize pyrolysis of the epoxide can act as a source of energetic O atoms that may be oxidizing the graphitic sheets also formed from the toluene solvent and covalently anchoring them to the NP surface (Figure 11b), thus requiring a higher temperature for exfoliation and oxidation (430 °C). It appears that the capping shell in this scenario, though more binding to the NP surface, is formed in lower quantities; the total mass loss (230−420 °C) is 32% versus 55% for the nonepoxide NPs. This is also apparent from the PXRD patterns, where a sizable broad peak is observed at 2θ 15−35° for the latter NPs (Figure S7, Supporting Information) that is

DOI: 10.1021/acs.inorgchem.5b00697
Inorg. Chem. 2015, 54, 5897−5906

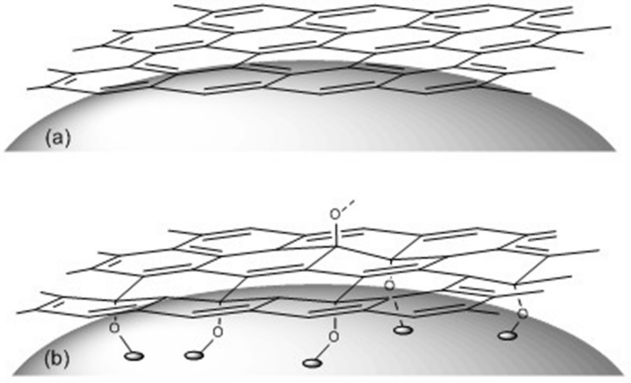

Figure 11. Capping of WC_{1-x} NP surfaces by EEW-pyrolyzed toluene in (a) the absence and (b) the presence of 1,2-epoxydodecane.

more intense compared with that for the epoxydodecane-capped NPs (Figure 7).

Table 3 shows a summary of all the oxide phases formed by oxidation of the metal and metal carbide NPs during DSC/TGA.

Table 3. Oxide Phases of Metals and Metal Carbide NPs Formed after Heating As Identified by PXRD[a]

metal/metal carbide	oxide phase	PDF card number
Co	Co_3O_4	00-043-1003
Ni	NiO	00-047-1049
Cu	CuO	01-080-1268
Pd	PdO	00-043-1024
Fe_5C_2	Fe_2O_3	01-079-0007
TiC	TiO_2	00-021-1276
WC_{1-x}	WO_3	00-043-1035
HfC	HfO_2	01-078-0049
NbC	$Nb_{16.8}O_{42}$	01-071-0336
ZrC	ZrO_2	01-080-0966

[a]PXRD patterns of the remaining oxide phases are shown in the Supporting Information (Figures S8−S10).

DISCUSSION

Carbide Formation Trends. Why do early transition metals form metal carbide NPs, while late transition metals form metal NPs under EEW conditions in organic solvents? We find a correlation with the enthalpy of formation (ΔH_f°) of the products. Metals that form carbides have negative enthalpies of formation, as shown in Table 4. Elements that do not form carbide NPs have corresponding metal carbides that are either explosive, highly unstable, not reported, or endoergic. This correlation suggests that product formation is driven by thermodynamic stability. This behavior is observed in all organic solvents used regardless of the ratio of C/H in the solvent. While EEW is a high-energy process, the change in product enthalpy should not be a strong function of temperature because metals and their carbides have low specific heats (Kirchoff's law).

NP Size Trends. We investigated the effects of solvent properties on the size of product NPs as measured by the Scherrer equation. Such analysis only allows a measure of the size of crystallite domains and does not provide a guarantee of the absence of polycrystallinity. Nevertheless we take these

Table 4. Enthalpies of Formation of Carbide Phases of Investigated Metals[a]

metal	EEW product	ΔH_f° carbide (kJ/mol)	metal oxidation state
Co	Co	39.04[b]	0
Ni	Ni	67.4	0
Cu	Cu	explosive[c]	0
Zn	Zn	no work[c]	0
Pd	Pd	NA[c]	0
Ag	Ag	unstable[c]	0
Ti	TiC	−184.1	+4
V	VC	−117.152[b]	+4
Fe	Fe_5C_2	NA	+1.6
Zr	ZrC	−207.1	+4
Nb	NbC	−138.9	+4
Mo	MoC	−28.5	+4
Hf	HfC	−226	+4
Ta	TaC	−144.1	+4
W	WC_{1-x}	−40.6 (WC)	+4(1−x)

[a]Taken from ref 55 unless otherwise indicated. [b]Taken from ref 56. [c]Taken from ref 57.

measurements as a good guide to the upper limit for individual NP diameters.

Previous studies have shown that immersion of a wire in a liquid during EEW reduces the product particle size by enhancing the deposited energy.[58] During the EEW process, the initial current travels along the surface of the wire. Under vacuum, the surface then begins to vaporize and form a plasma state, which provides a low-resistance medium for conduction of current. This minimizes energy deposition into the core of the wire and results in larger particles. In the presence of a liquid medium the surface plasma is significantly suppressed, forcing more energy into the core of the wire. We see smaller particles formed when the wire is immersed in a liquid than when the wire is exposed to argon.[59,60] Figure 12 shows the sizes of different metals produced by EEW, and we can see that all sizes are ≤30 nm. Indeed most of the metal NPs fall within the 10−15 nm range.

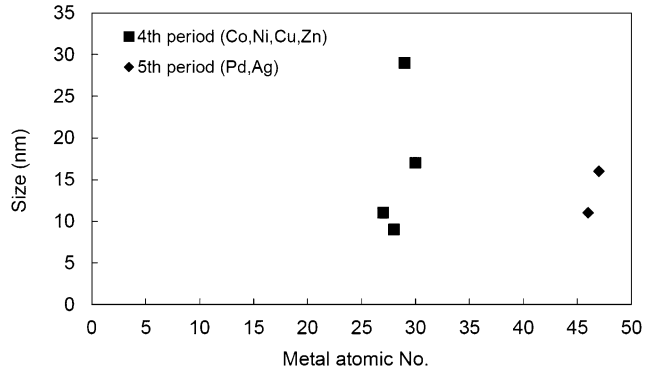

Figure 12. PXRD/Scherrer sizes of metallic NPs produced by EEW in toluene.

Sizes of metal carbide NPs also were on the order of ≤30 nm, which are similar to sizes produced from metallic NPs synthesized under the same conditions of EEW as shown in Figure 13. We can see that the sizes are comparable in both toluene and benzene. Therefore, solvent variation has no effect on metal carbide core sizes.

DOI: 10.1021/acs.inorgchem.5b00697
Inorg. Chem. 2015, 54, 5897−5906

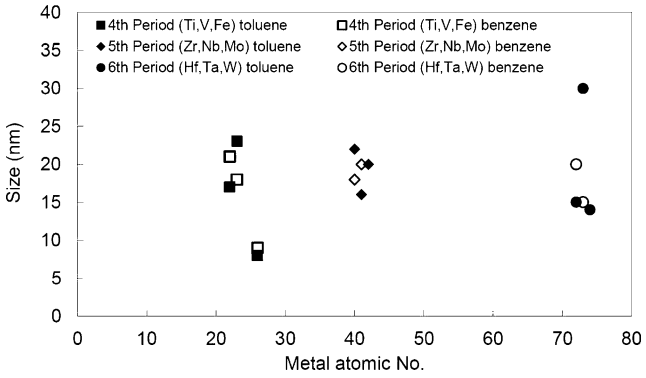

Figure 13. PXRD/Scherrer sizes of metal carbide NPs produced by EEW in toluene or benzene.

Capping Trends. Metal NPs have many interesting applications. However, production of metal NPs presents unique challenges due to their instability in atmospheric conditions. For these metals, it is reported that there is neither a kinetic nor a thermodynamic barrier to agglomeration.[61] Surface capping is used to overcome this problem by arresting the growth of NPs at their initial stage. Without preventing agglomeration of the NPs produced, they will come in contact and grow rapidly to form bigger particles and eventually bulk material. Additionally, some metal NPs are reactive with atmospheric constituents and must be passivated to allow ease of handling and use.

Previously a polyether cap was observed as a very effective method to stabilize aluminum NPs. The polyether was formed by reaction of the nascent Al NP with epoxides.[62] In that study, Al NPs were produced by decomposition of alane precursor. The organic capping layer was generated by reaction of the incipient Al NPs with the epoxide monomer by PIERMEN. Electron-rich metals such as Al and Na can work as initiators to cause ring opening of epoxides, leading to the formation of transient surface alkoxide carbanions.[63,64] These structures can bind to the metal surface via the oxygen, and propagation ensues by carbanionic attack on the next epoxide monomer. A putative alkane-dioxy loop will be created and would grow to create polyether loops from the metal core surface. Longer epoxide alkyl side chains provide a hydrophobic environment around the NP core, affording resistance to diffusion by small molecules such as oxygen and water, in particular.

Aluminum and sodium are stronger reducing agents than Zn or Fe, and Na as well as Al NPs were successful in ring opening of epoxides. We have looked at which point the metal reduction potential might be a limiting factor in whether or not epoxides could be ring-opened leading to polymerization of the nascent metal NP surface. Such passivation using 1,2-epoxydodecane can be probed by ATR-FTIR spectroscopic measurements of the isolated metal NPs, which reveal an increased absorption at around 1050 cm^{-1} for the C−O−C stretch, which is quite distinct for the parent epoxide (1250 cm^{-1}). Typical spectra for Ni and Co are shown in Figure 14.

The capped NPs were air-stable, which can be attributed to the effective passivation and formation of a polyether layer, which limits the permeability to molecular atmospheric constituents. Thus, PIERMEN is demonstrated to be effective in preventing the self-ignition of bare metal NPs. However, not all metals were successful in opening the epoxide ring. It was observed that there is a well-defined threshold polarographic half-wave potential, above which the metal is not sufficiently

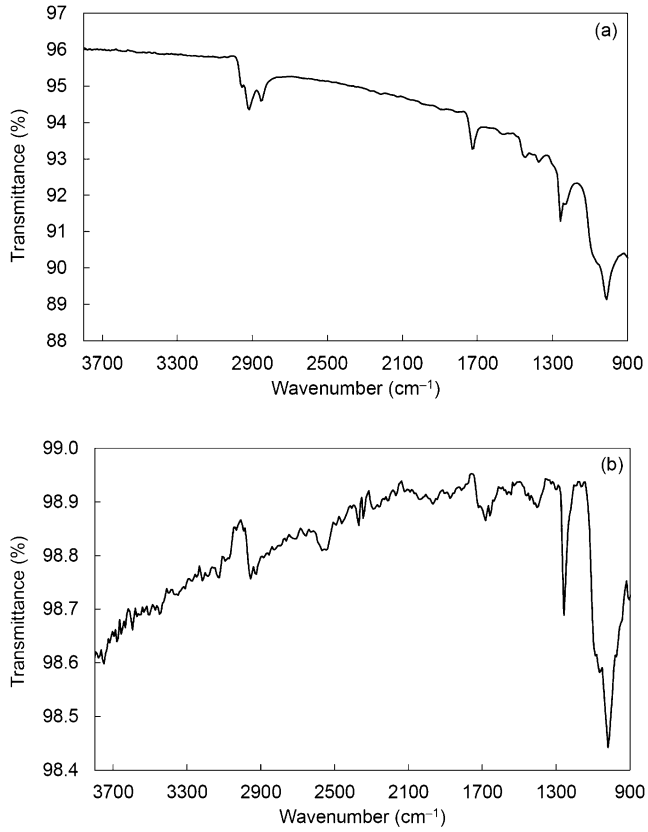

Figure 14. IR spectra of (a) Ni NPs and (b) Co NPs capped with 1,2-epoxydodecane. Such polyether formation has also been observed by us in EEW synthesis of Zn NPs.[36]

reducing to cause epoxide ring opening. Table 5 shows the different metals (that form metal NPs exclusively) with their

Table 5. Polarographic Half-Wave Potentials of Metallic NPs in THF Relative to Bis(biphenyl) Chromium(I)/(0)[a]

metal	standard reduction potential, $E°$ (V)	epoxide ring opening
Zn	−0.049	successful
Co	−0.420	successful
Ni	−0.453	successful
Cu	0.817	unsuccessful
Ag	1.297	unsuccessful
Pd	NA	unsuccessful

[a]Taken from ref 65.

potential values (Zn, Co, Ni), and we can see that metals with negative potentials can induce ring opening, while metals with positive values (Cu, Ag, Pd) were not successful at initiating the epoxide ring-opening process.

CONCLUSIONS

Different metal and metal carbide NPs were produced using EEW coupled with 1,2-epoxydodecane as a precursor for NP capping and stabilization. All NPs were capped and air-stable with particle core sizes less than 30 nm. PXRD confirms the crystalline phases of products, while TEM shows NPs embedded in an organic cap matrix. Metal carbide NPs are observed for those elements where the corresponding metal carbide enthalpy of formation is negative. Thermodynamic stability was the driving force behind formation of metal

DOI: 10.1021/acs.inorgchem.5b00697
Inorg. Chem. 2015, 54, 5897−5906

carbides for early transition metals (groups 4−8) compared to late transition metals (groups 9−12).

■ ASSOCIATED CONTENT

Supporting Information

PXRD patterns of metal and metal carbide NPs as well as resulting metal oxides produced by DSC/TGA analysis. The Supporting Information is available free of charge on the ACS Publications website at DOI: 10.1021/acs.inorgchem.5b00697.

■ AUTHOR INFORMATION

Corresponding Authors

*E-mail: jellissp@slu.edu.
*E-mail: buckners@slu.edu.

Notes

The authors declare no competing financial interest.

■ ACKNOWLEDGMENTS

Acknowledgement is made to the National Science Foundation for support under grant CHE-0963363 for renovations to the research laboratories in Monsanto Hall at Saint Louis University.

■ REFERENCES

(1) Li, P. G.; Lei, M.; Tang, W. H. *Mater. Res. Bull.* **2008**, *43*, 3621−3626.
(2) Enayati, M. H.; Seyed-Salehi, M.; Sonboli, A. *J. Mater. Sci.* **2007**, *42*, 5911−5914.
(3) Kim, J. C.; Kim, B. K. *Scr. Mater.* **2004**, *50*, 969−972.
(4) Shapoval, V. I.; Malyshev, V. V.; Tishchenko, A. A.; Kushkhov, K. B. *Inorg. Mater.* **2000**, *36*, 1020−1023.
(5) Hyeon, T.; Fang, M.; Suslick, K. S. *J. Am. Chem. Soc.* **1996**, *118*, 5492−5493.
(6) Hassine, N. A.; Binner, J. G. P.; Cross, T. E. *Int. J. Refract. Met. Hard Mater.* **1995**, *13*, 353−358.
(7) Nazarenko, O. B. *Glass Ceram.* **2005**, *62*, 364−367.
(8) Kotov, Y. *Adv. Sci. Technol.* **2003**, *30*, 381−388.
(9) Leopold, H. S. Effect of bridgewire parameters on explosive initiation. In *Exploding Wires, Volume 3: Proceedings of the Third Conference on the Exploding Wire Phenomenon*, Boston, 1964; Plenum Press, 1964; pp 125−152.
(10) Romanova, V.; Tkachenko, S.; Mingaleev, A.; Agafonov, A.; Ter-Oganesyan, A.; Shelkovenko, T.; Pikuz, S. *AIP Conf. Proc.* **2009**, *1088*, 176−179.
(11) Ostrovskaya, G. V. *Technol. Phys.* **2008**, *53*, 1103−1128.
(12) Phalen, R. F. *J. Aerosol Sci.* **1972**, *3*, 395−409.
(13) Kotov, Y. A. *Nanotechnol. Russ.* **2009**, *4*, 415−424.
(14) Yoon-Cheol, H.; Chuhyun, C. *J. Korean Phys. Soc.* **2010**, *57*, 1574−1576.
(15) Cho, C.; Choi, Y.-W.; Jiang, W. *J. Korean Phys. Soc.* **2005**, *47*, 987−990.
(16) Gromov, A. A.; Foerter-Barth, U.; Teipel, U. *Powder Technol.* **2006**, *164*, 111−115.
(17) Kinemuchi, Y.; Sato, K.; Watari, K.; Cho, C.; Murai, K.; Suematsu, H.; Jiang, W.; Yatsui, K. *J. Ceram. Soc. Jpn.* **2004**, *112*, 355−362.
(18) Kotov, Y. A.; Azarkevich, E. I.; Beketov, I. V.; Demina, T. M.; Murzakaev, A. M.; Samatov, O. M. *Key Eng. Mater.* **1997**, *132−136*, 173−176.
(19) Kinemuchi, Y.; Murai, K.; Sangurai, C.; Cho, C.-H.; Suematsu, H.; Jiang, W.; Yatsui, K. *J. Am. Ceram. Soc.* **2003**, *86*, 420−424.
(20) Hokamoto, K.; Wada, N.; Tomoshige, R.; Kai, S.; Ujimoto, Y. *J. Alloys Compd.* **2009**, *485*, 573−576.
(21) Kim, W.; Park, J.-s.; Suh, C.-y.; Cho, S.-w.; Lee, S. *Mater. Trans.* **2009**, *50*, 2344−2346.
(22) Yun, J.-Y.; Lee, H.-M.; Choi, S.-Y.; Yang, S.; Lee, D.-W.; Kim, Y.-J.; Kim, B.-K. *Mater. Trans.* **2011**, *52*, 250−253.
(23) Yoon-Cheol, H.; Chuhyun, C.; Young-Ugk, K.; Hun-Joon, S. *J. Korean Phys. Soc.* **2011**, *59*, 3458−3462.
(24) Debalina, B.; Kamaraj, M.; Murthy, B. S.; Chakravarthi, S. R.; Sarathi, R. *J. Alloys Compd.* **2010**, *496*, 122−128.
(25) Suematsu, H.; Minami, C.; Kobayashi, R.; Kinemuchi, Y.; Hirata, T.; Hatakeyama, R.; Yang, S.-C.; Jiang, W.; Yatsui, K. *Jpn. J. Appl. Phys., Part 2* **2003**, *42*, L1028−L1031.
(26) Kobayashi, R.; Suematsu, H.; Suzuki, T.; Jiang, W.; Yatsui, K. *Trans. Mater. Res. Soc. Jpn.* **2003**, *28*, 441−443.
(27) Kotov, Y. A.; Azarkevich, E. I.; Medvedev, A. I.; Murzakaev, A. M.; Kuznetsov, V. L.; Samatov, O. M.; Demina, T. M.; Timoshenkova, O. R.; Shtoltz, A. K. *Inorg. Mater.* **2007**, *43*, 633−637.
(28) Cho, C.; Ha, Y.-C.; Kang, C.; Jin, Y.-S.; Rim, G.-H. *Jpn. J. Appl. Phys.* **2011**, *50*, 106201/1−106201/4.
(29) Chuhyun, C.; Yoon-Cheol, H.; Chungil, K.; Yun-Sik, J.; Geun-Hie, R. *J. Korean Phys. Soc.* **2010**, *57*, 1807−1810.
(30) Johnson, R. L.; Siegel, B. *J. Electrochem. Soc.* **1968**, *115*, 24−28.
(31) Ilyin, A. P.; Nazarenko, O. B.; Tikhonov, D. V. *J. Nanosci. Nanotechnol.* **2012**, *12*, 8137−8142.
(32) Yu, X.; Chai, Y.; Jiang, J.; Cui, H. *J. Photochem. Photobiol. A* **2012**, *241*, 45−51.
(33) Oh, J. Y.; Choi, H. S.; Kim, M. S.; Kim, Y. S.; Park, C. R. *J. Mater. Res.* **2012**, *27*, 2035−2045.
(34) Johnson, B. F. G. *Top. Catal.* **2003**, *24*, 147−159.
(35) Kwon, Y. S.; Gromov, A. A.; Ilyin, A. P.; Ditts, A. A.; Kim, J. S.; Park, S. H.; Hong, M. H. *Int. J. Refract. Met. Hard Mater.* **2004**, *22*, 235−241.
(36) Abdelkader, E. M.; Jelliss, P. A.; Buckner, S. W. *Mater. Chem. Phys.* **2015**, *149−150*, 238−245.
(37) Pachón, L. D.; Rothenberg, G. *Appl. Organomet. Chem.* **2008**, *22*, 288−299.
(38) Reetz, M. T.; Helbig, W. *J. Am. Chem. Soc.* **1994**, *116*, 7401−7402.
(39) Fukuoka, A.; Sato, A.; Kodama, K.-y.; Hirano, M.; Komiya, S. *Inorg. Chim. Acta* **1999**, *294*, 266−274.
(40) Del Angel, P.; Dominguez, J. M.; Del Angel, G.; Montoya, J. A.; Lamy-Pitara, E.; Labruquere, S.; Barbier, J. *Langmuir* **2000**, *16*, 7210−7217.
(41) Kalyan Kamal, S. S.; Sahoo, P. K.; Premkumar, M.; Rama Rao, N. V.; Jagadeesh Kumar, T.; Sreedhar, B.; Singh, A. K.; Ram, S.; Chandra Sekhar, K. *J. Alloys Compd.* **2009**, *474*, 214−218.
(42) Yılmaz, F.; Lee, D.-J.; Song, J.-W.; Hong, H.-S.; Son, H.-T.; Yoon, J.-S.; Hong, S.-J. *Powder Technol.* **2013**, *235*, 1047−1052.
(43) Singla, M. L.; Negi, A.; Mahajan, V.; Singh, K. C.; Jain, D. V. S. *Appl. Catal. A: Gen.* **2007**, *323*, 51−57.
(44) Aravinth, S.; Sankar, B.; Kamaraj, M.; Chakravarthy, S. R.; Sarathi, R. *Inter. J. Refract. Met. Hard Mater.* **2012**, *33*, 53−57.
(45) Li, Z.-Y.; Yuan, Z.; Zhao, Y.-X.; He, S.-G. *Chem.—Eur. J.* **2014**, *20*, 4163−4169.
(46) Armentrout, P. B. *Annu. Rev. Phys. Chem.* **1990**, *41*, 313−344.
(47) Armentrout, P. B.; Beauchamp, J. L. *J. Am. Chem. Soc.* **1981**, *103*, 784−791.
(48) Armentrout, P. B. *Int. J. Mass Spectrom.* **2000**, *200*, 219−241.
(49) Pope, R. M.; VanOrden, S. L.; Cooper, B. T.; Buckner, S. W. *Organometallics* **1992**, *11*, 2001−2003.
(50) Pope, R. M.; Buckner, S. W. *Org. Mass Spectrom.* **1993**, *28*, 1616−1621.
(51) Buckner, S. W.; MacMahon, T. J.; Byrd, G. D.; Freiser, B. S. *Inorg. Chem.* **1989**, *28*, 3511−3518.
(52) Boehme, D. K.; Schwarz, H. *Angew. Chem., Int. Ed.* **2005**, *44*, 2336−2354.
(53) Irikura, K. K.; Beauchamp, J. L. *J. Am. Chem. Soc.* **1991**, *113*, 2769−2770.
(54) Ilyin, A. P.; Nazarenko, O. B. *J. Optoelectron. Adv. Mater.* **2007**, *9*, 1521−1524.

DOI: 10.1021/acs.inorgchem.5b00697
Inorg. Chem. 2015, 54, 5897−5906

(55) Binnewies, M.; Milke, E. Data Section A. In *Thermochemical Data of Elements and Compounds*; Wiley-VCH Verlag GmbH, 2008; pp 11−87.
(56) Wicks, C. E.; Block, F. E. *Bull. - U. S., Bur. Mines* **1963**, *605*, 146.
(57) Shatynski, S. R. *Oxid. Met.* **1979**, *13*, 105−118.
(58) Cho, C.; Choi, Y. W.; Kang, C.; Lee, G. W. *Appl. Phys. Lett.* **2007**, *91*, 141501/1−141501/3.
(59) Yun, G. S.; Bac, L. H.; Kim, J. S.; Kwon, Y. S.; Choi, H. S.; Kim, J. C. *J. Alloys Compd.* **2011**, *509*, S348−S352.
(60) Chuhyun, C.; Chungil, K.; Yun-Cheol, H.; Yoon-Sik, J.; Geun-Hie, R. *J. Korean Phys. Soc.* **2011**, *59*, 3662−3665.
(61) Haber, J. A.; Buhro, W. E. *J. Am. Chem. Soc.* **1998**, *120*, 10847−10855.
(62) Chung, S. W.; Guliants, E. A.; Bunker, C. E.; Hammerstroem, D. W.; Deng, Y.; Burgers, M. A.; Jelliss, P. A.; Buckner, S. W. *Langmuir* **2009**, *25*, 8883−8887.
(63) Hammerstroem, D. W.; Burgers, M. A.; Chung, S. W.; Guliants, E. A.; Bunker, C. E.; Wentz, K. M.; Hayes, S. E.; Buckner, S. W.; Jelliss, P. A. *Inorg. Chem.* **2011**, *50*, 5054−5059.
(64) Thomas, B.; Bunker, C.; Guliants, E.; Hayes, S.; Kheyfets, A.; Wentz, K.; Buckner, S.; Jelliss, P. *J. Nanopart. Res.* **2013**, *15*, 1−9.
(65) Gritzner, G. *Pure Appl. Chem.* **1990**, *62*, 1839−1858.

DOI: 10.1021/acs.inorgchem.5b00697
Inorg. Chem. 2015, 54, 5897−5906